Supplement of

Contribution of Lakes in Sustaining Greening of the Sahara during the Mid-Holocene

Yuheng Li[1], Kanon Kino[1], Alexandre Cauquoin[2] and Taikan Oki[1]

[1]Department of Civil Engineering, Graduate School of Engineering, the University of Tokyo, Tokyo, Japan.

[2]Institute of Industrial Science, The University of Tokyo, Kashiwa, Japan.

Correspondence to: Yuheng Li (yuheng@rainbow.iis.u-tokyo.ac.jp)

Contents of this file

Table S1.

Table S1 Lake Maps

Lake Maps	Spatial resolution of original lake reconstruction	Description	Reference
MH_98 (small-lake map)	160 km	Holocene small-lake fraction derived from paleo-ecological reconstructions	(Hoelzmann, Jolly et al., 1998)
MH_02 (potential maximum-lake map)	160 km	mid-Holocene maximum-lake fraction derived using the hydrological routing algorithm (HYDRA)	(Tegen, Harrison et al., 2002)
MH1, MH2, MH3, MH4	15 arc-second	RFM2 model results on the wetlands of North Africa during the mid-Holocene corresponding to the four different rainfall types (MH1-4). The MH1 and MH2 are derived from IPSL-CM6A-LR mid-Holocene simulation; MH3 and MH4 are based on EC-Earth mid-Holocene simulation	(Chen, Ciais et al., 2021)

Considering the different spatial resolutions of the above datasets, the input lake maps have been upscaled into T42 spatial resolutions by calculating the lake area grid proportion in each T42 grid in North Africa Areas. Besides, this study used the same MH_98 and MH_02 maps as that of Specht, Claussen et al. (2022), which have been published in *http://hdl.handle.net/21.11116/0000-0009-63B5-B*.

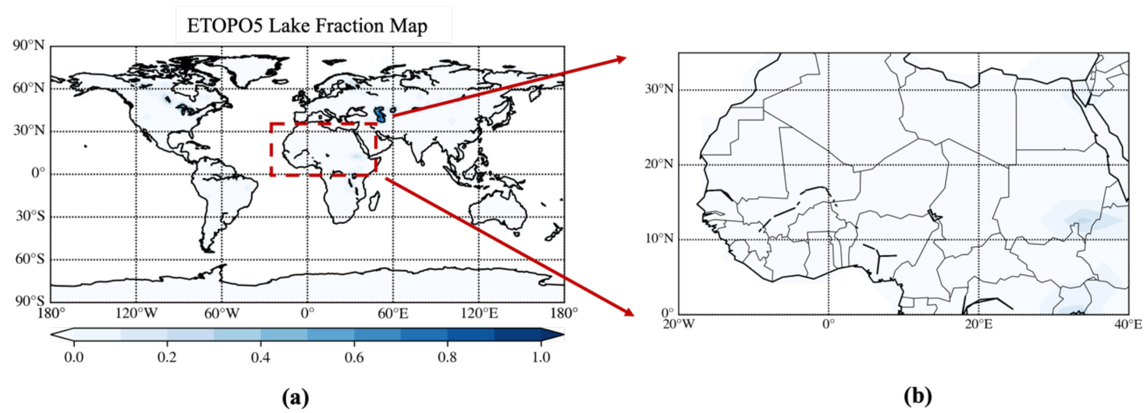

Figure S1. The (a) global prescribed lake map for mid-Holocene (MH) and pre-industrial (PI) reference experiments (ETOPO5). (b) Focus over North Africa.

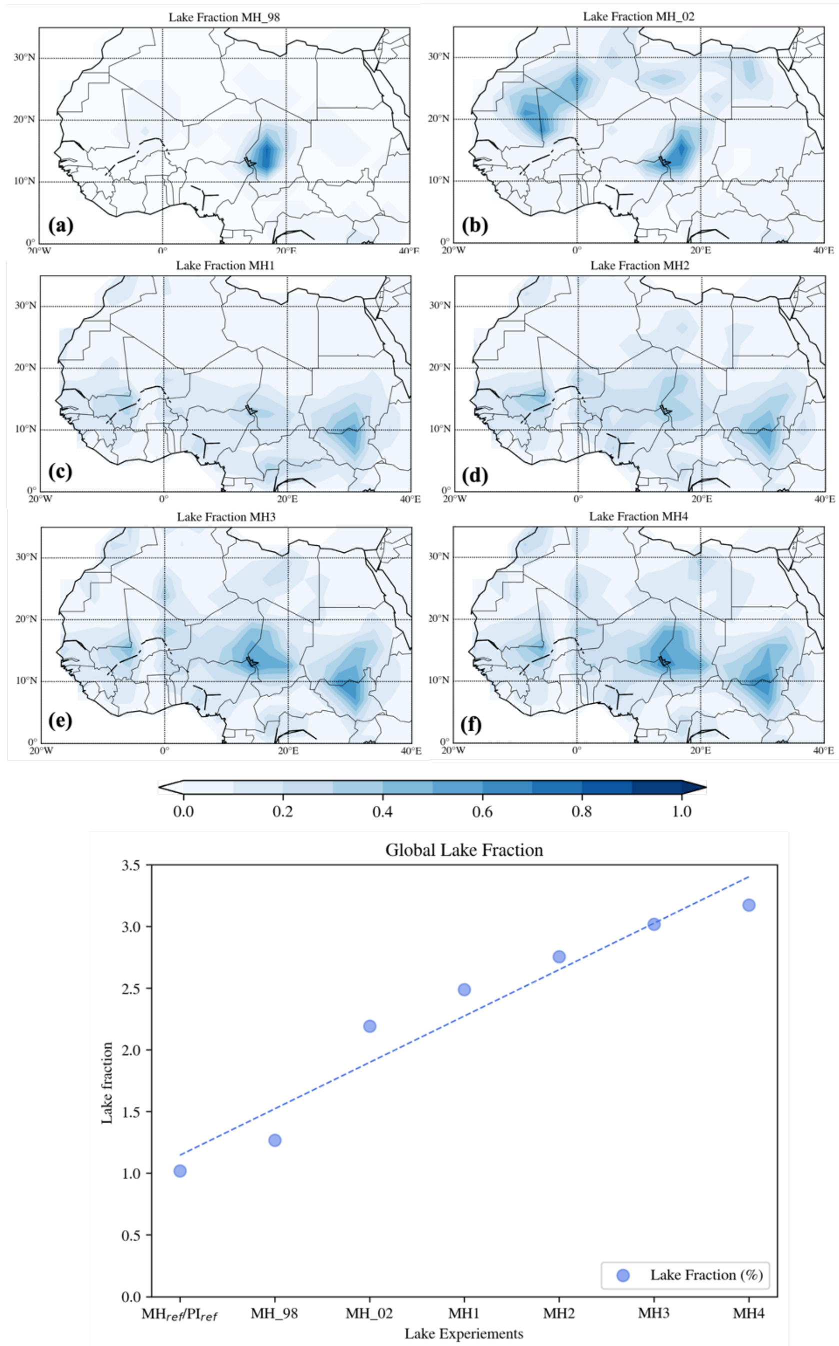

Figure S2. The mid-Holocene (MH) lake maps in northern Africa used in this study: (a) the small lake map derived by (Hoelzmann, Jolly et al., 1998) used for the MH_C experiments, (b) the maximum lake map derived by Tegen, Harrison et al. (2002) used for the MHWC experiments, (c)-(f) the potential lake maps derived by Chen, Ciais et al. (2021) corresponding to four different types of precipitation, used for the MH_{WCE1}, MH_{WCE2}, MH_{WCE3} and MH_{WCE4} experiments, respectively. The lake maps differences mainly come from the western Sahara lakes, Megalake Chad and eastern lakes in South Sudan (between 0°-20°N). (g) The fraction (circle size) of all the prescribed lakes experiments compared with the present global land surface areas (1.48 $\times 10^8$ km2).

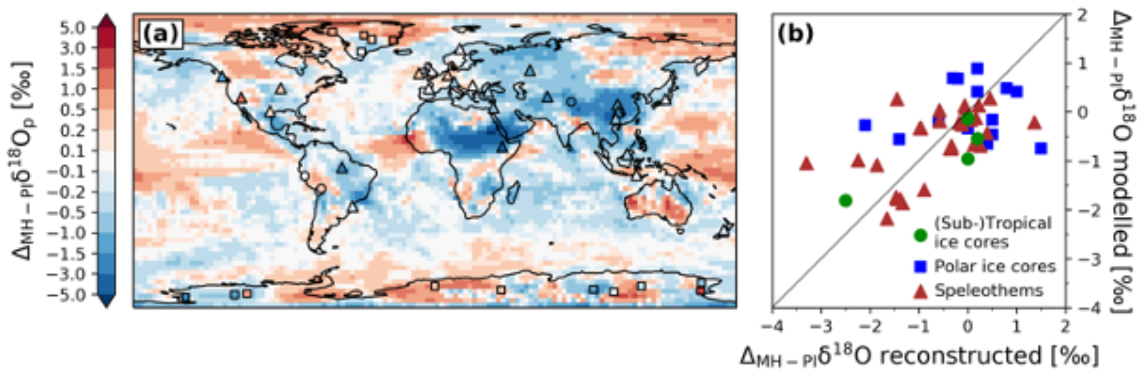

Figure S3. Isotope model-data comparison for the reference mid-Holocene simulation. The subplot (a) shows the simulated global pattern of annual mean $\delta^{18}O_p$ changes in precipitation between the MH_{ref} and PI_{ref} climate (background colors) and the observed $\delta^{18}O$ changes in polar (squares) and (sub)tropical (dots) ice cores and in calcite speleothems. The subplot (b) is a scatter plot showing a comparison of observed δ18O changes from ice cores and speleothems vs. with simulated MH–PI δ18Op anomalies at the same location.

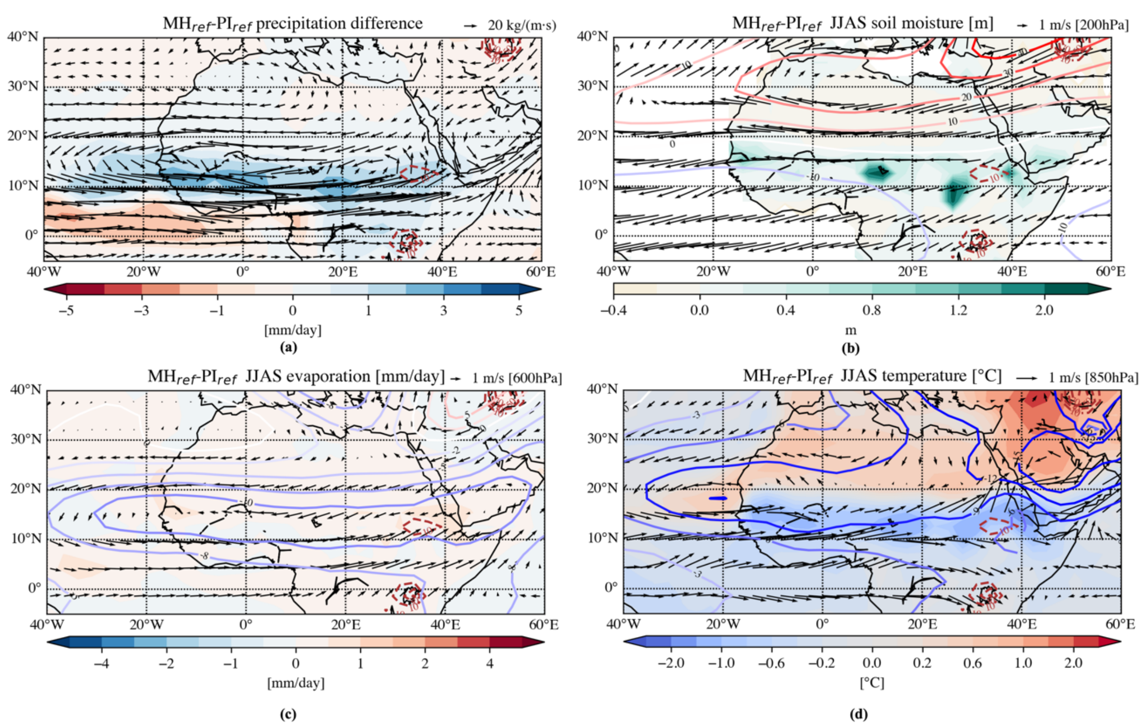

Figure S4. The simulated climatological mean anomalies between MHref and PIref in JJAS: (a) precipitation (shades) and the integrated vapor transportation anomalies (IVT; arrows); (b) soil moisture (shades) with 200 hPa wind (arrows) and geopotential height (contours); (c) evaporation (shades) with and 600 hPa horizontal wind (arrows) and geopotential height (contours); (d) surface temperature (shades) with 850 hPa horizontal wind (arrows), and geopotential height (contours). For (a)-(d), the lake fraction [%] contours of the respective lake sensitivity experiment are shown with the red dashed lines, and the respective reference scale for the arrow is shown at the right top of each panel.

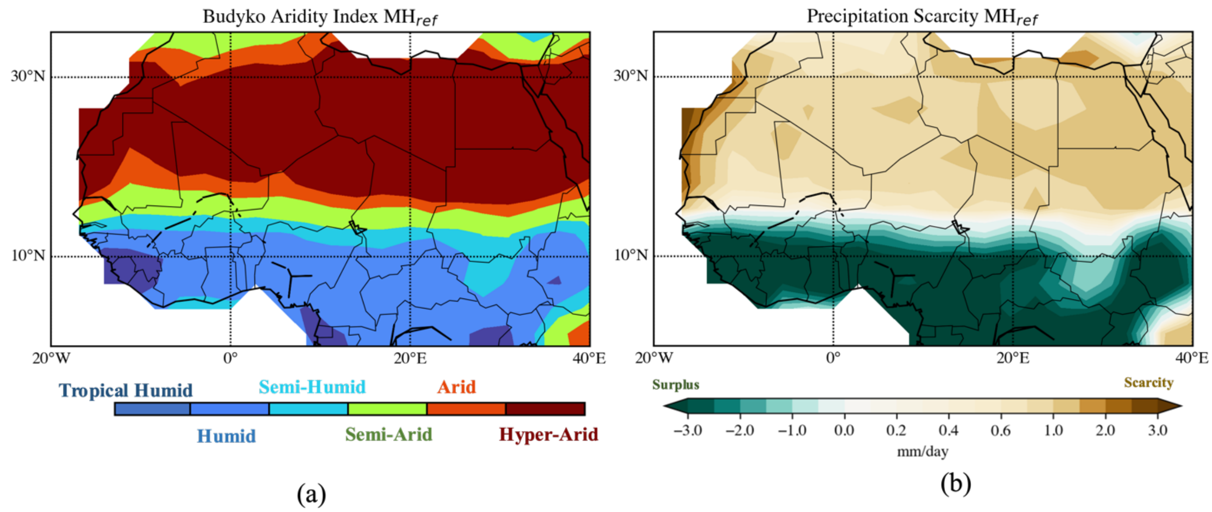

Figure S5. (a) The spatial distribution of precipitation scarcity and precipitation surplus over Northern Africa and (b) the spatial distribution of six climate regions for MH$_{\mathrm{ref}}$ experiments.

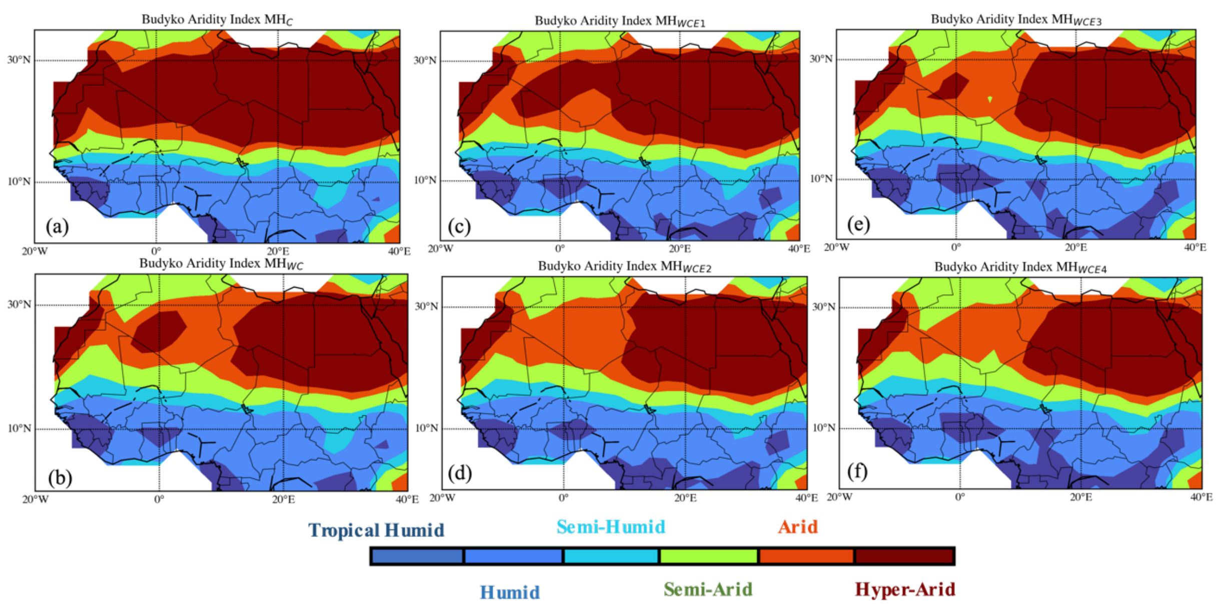

Figure S6. The spatial distribution of six climate regions for MH$_{C}$, MH$_{WC}$, MH$_{WCE1}$, MH$_{WCE2}$, MH$_{WCE3}$, and MH$_{\mathrm{WCE4}}$ experiments. The climate zones are classified with Budyko Aridity index (I) and precipitation (P) in Northern Africa: Tropical Humid ($I \leqslant 0.7$ and $P > 2{,}000$ mm/yr), Humid ($0.7 < I \leqslant 1.2$), Semi-Humid ($1.2 < I \leqslant 2.0$), Semi-Arid ($2.0 < I \leqslant 4.0$), Arid ($4.0 < I \leqslant 6.0$) and Hyper-Arid ($6.0 < I$). For Budyko Aridity index calculation, see the main text in method detail.

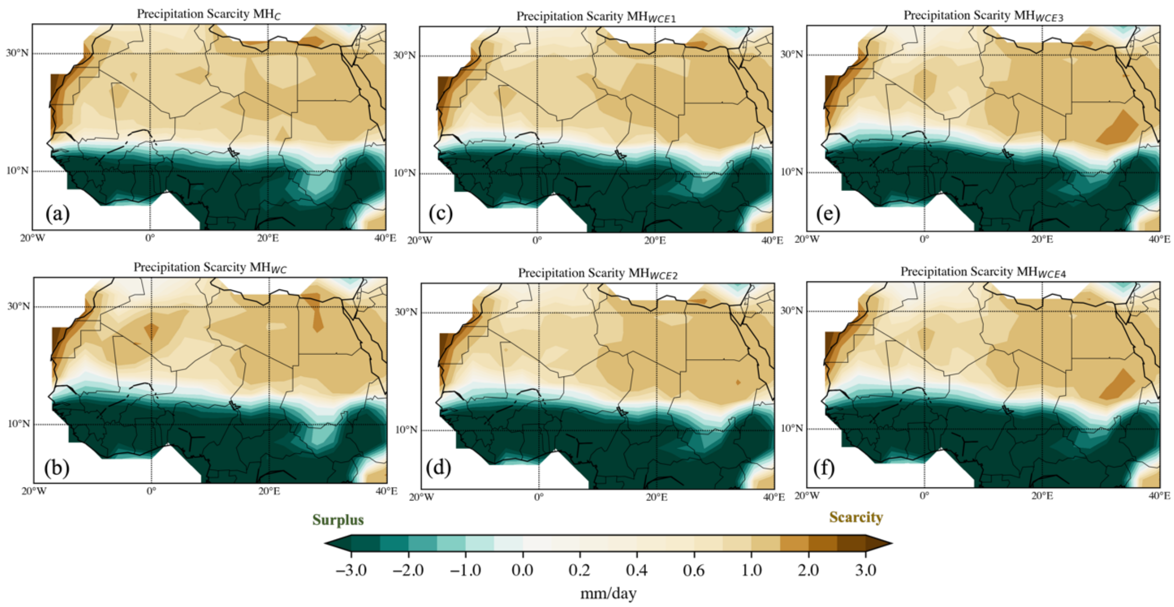

Figure S7. The spatial distribution of precipitation scarcity and precipitation surplus over Northern Africa for all the mid-Holocene experiments.

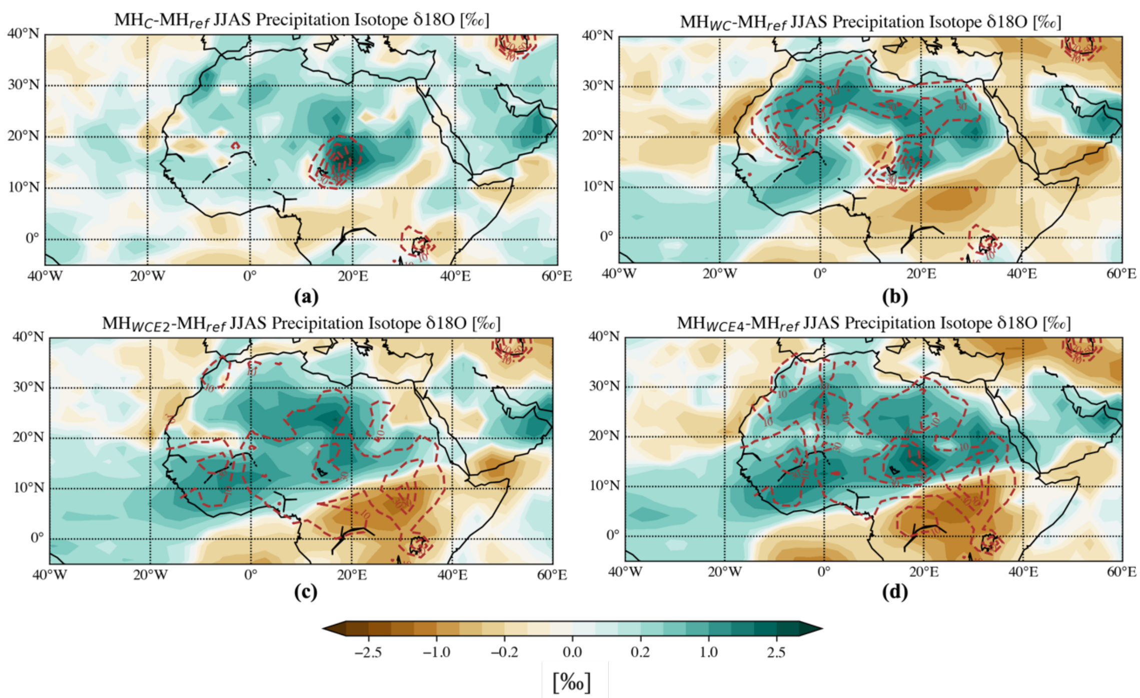

Figure S8. Changes in the stable isotope ratio $\delta^{18}O$ [‰] in precipitation for our mid-Holocene sensitivity experiments relative to MH_{ref}: (a) the climatological δ18O anomaly for MH_98 experiments. (b), (c) and (d) are the same as (a) but for the MH_{WC}, MH_{WCE2} and MH_{WCE4} experiments, respectively. For (a)-(d), the lake fraction [%] contours of the respective lake sensitivity experiment are shown with the red dashed lines.